High-order finite beam elements for propagation analyses of arbitrary-shaped one-dimensional waveguides

High-order finite beam elements for propagation analyses of arbitrary-shaped one-dimensional waveguides

Matteo Filippi
Assistant Professor, Ph.D.
matteo.filippi@polito.it
Alfonso Pagani
Associate Professor, Ph.D.
alfonso.pagani@polito.it
Erasmo Carrera
Full Professor, Ph.D.
erasmo.carrera@polito.it
Department of Mechanical and Aerospace Engineering
MUL^2 research group, www.mul2@polito.it
Politecnico di Torino, Torino, Italy

Abstract

This paper presents advanced kinematic beam models to compute the dispersion characteristics of one-dimensional guides. High-order functions are used to interpolate the primary variables above the waveguide cross-section and along its axis. Taylor- and Lagrange-type bi-dimensional expansions are employed to describe the section deformation, while Lagrangian shape functions approximate the displacement field along the propagating direction. According to the Wave Finite Element Method, the stiffness and mass matrices corresponding to various structural theories are post-processed to build the transfer matrix of a representative waveguide portion. The Carrera Unified Formulation is exploited to calculate these matrices.

keywords: dispersion analyses; periodic structures; waveguide; WFEM; advanced finite beam element; Floquet-Bloch theory

1. Introduction

The wave propagation problem is of great interest in several engineering fields. The knowledge of energy transfer mechanisms through structural components enables one to predict the level of acoustic emissions and vibrations and, whenever possible, conceive strategies to reduce them. The related literature is vast and includes studies based on analytical, semi-analytical, and numerical approaches. Analytical solutions, which are often referred to as exact solutions, are available only for simple waveguide geometries such as thin rods, beams with compact cross-sections, membranes, thin plates, and shells [1]. Such relations rely on simplified stress and strain fields that are not (in general) representative for complex structures. Thus, arbitrary-shaped waveguides must be examined by utilizing either semi-analytical or numerical techniques. The adjective semi-analytical implies that the wavefield is somehow described exactly, by assuming harmonic displacement variations along the propagating direction. Among others, the Dynamic Stiffness (DS) method allows one to derive exact elemental dynamic stiffness matrices that can be assembled to analyze complicated geometries, similarly to the Finite Element (FE) method. Wave modes, namely the deformation modes of the waveguide, can be calculated with different kinematic fields. One- and two-dimensional DS formulations were developed by adopting the Euler-Bernoulli, Timoshenko, Mindlin, and Reddy's models [2, 3, 4, 5], and arbitrary-order structural theories [6]. The problem deriving from the DS formulation is nonlinear, and its solution requires iterative algorithms to calculate natural frequencies and eigenmodes. Other semi-analytical approaches exploit the FE method advantages by conceiving specific approximating functions. For example, Doyle [7] introduced the concept of *dynamic shape function* to simulate the harmonic variations of primary variables between two or more nodes. These functions are defined in the Fourier domain, therefore they are frequency-dependent and complex-valued. This finite element formulation, also referred to as the Fast Fourier Transform (FFT)-based Spectral Finite Element (SFE) method, allows one to predict the dynamic structural response at high frequencies with few elements [8] since the inertial effect is being described exactly. However, the FFT-SFE method has been mainly utilized to develop low-order finite elements due to the difficult derivation of dynamic shape functions for arbitrary kinematic theories [9, 8, 10]. An alternative FE-based technique uses orthogonal polynomials, such as Lagrange, Chebyshev, and Legendre expansions, to derive p-version elements whose or-

der can be selected according to the considered frequency range. Such an approach was employed to develop solid [11, 12], plate [13], and advanced beam [14] elements. Other spectral solutions conceptually different from the above methodologies were obtained by meshing the section waveguide with finite elements and adopting analytic solutions along the propagation directions. The FE discretization performed with both conventional [15, 16] and spectral formulations [17, 18] enables the detection of many mode shapes and the analysis of complex waveguides.

The Wave Finite Element (WFE) method is undoubtedly one of the most powerful techniques to analyze periodic waveguides. The methodology enables calculating a structural member's dispersion characteristics by only discretizing a small part of its domain. Bloch periodic conditions are applied by postprocessing the representative segment's dynamic stiffness matrix. The WFE method offers two prominent advantages with respect to other spectral techniques, namely the possibility of using standard FE packages and the reduction of the mathematical domain to be discretized. This approach was applied to investigate free and forced vibrations of one- and two-dimensional waveguides with prismatic sections such as thin-walled structures [19, 20, 21], fluid-filled pipes [22], laminates, and sandwich configurations [23, 24, 25, 26]. Furthermore, other applications studied multi-section waveguides to obtain either dispersion characteristics of stiffened structures [27] or metastructures pass/stop bands [28, 29, 30, 31]. The literature review reveals that periodic segments with complex and highly deformable sections are usually modeled with either plates or brick elements to capture as many wave modes as possible. In contrast, beam elements are adopted when the waveguide section experiences rigid bending, longitudinal and torsional deformations.

This paper aims at employing advanced finite beam elements within the WFE framework to investigate the propagation mechanisms of one-dimensional guides. The Carrera Unified Formulation (CUF) is utilized to derive the dynamic stiffness matrices of the waveguide portion related to arbitrary kinematic theories. The finite element mesh is placed along the propagation direction of waves, while the displacement field above the guide cross-section is approximated with Taylor- and Lagrange-type bi-dimensional polynomials. The FE shape functions are one-dimensional Lagrangian functions of the axial coordinate, whose orders depend on the number of element nodes. Linear, quadratic, and cubic approximations are obtained by utilizing beam elements with two, three, and four nodes, respectively. With the Taylor expansions, the displacement field can be enriched in a spectral sense by

merely raising the polynomial degree. The Lagrange approach enables one to refine the kinematic description by increasing either the polynomial order or the number of subdomains utilized to model the waveguide section. The CUF-based beam elements were quite extensively adopted for the analysis of composite structures [32, 33], aerospace constructions [34, 35], and many other applications, including rotor-dynamics [36, 37] and multifield problems [38, 39]. Comparisons with analytical and standard FE solutions reported in the mentioned works demonstrate the computational efficiency and the significant level of accuracy that can be achieved with CUF elements. The next section briefly reviews the WFE method and the unified formulation and then dispersion diagrams of three one-dimensional waveguides obtained with different kinematic theories are reported and discussed.

2. Theoretical section

The WFE method makes use of standard FE matrices for modeling the wave propagation mechanisms throughout one or more spatial directions and its implementation is rather straightforward. Figure 1 schematically shows the modelization of a waveguide portion, whose lenght is assumed to be equal to Δ.

According to the unified formulation, the displacement field $\mathbf{u}^T = (u_x\, u_y\, u_z)^T$, which is function of the three spatial coordinates (x, y, z) and time (t), is written as

$$\mathbf{u}(x, y, z, t) = F_\tau(x, z) N_i(y) \mathbf{q}_{i\tau}(t) \qquad 1 \leq i \leq ne \qquad 1 \leq \tau \leq M \qquad (1)$$

where $F_\tau(x, z)$ and $N_i(y)$ are functions defined above the waveguide section and along its perpendicular direction, respectively. The vector $\mathbf{q}_{i\tau}(t)$ collects the nodal generalized coordinates for each pair of τ and i indexes. Terms $N_i(y)$ are the Lagrangian shape functions [40] defined along each finite beam element used to discretize the segment. The polynomial degree depends on the number of structural nodes (ne) belonging to the beam element. Linear, quadratic, and cubic elements are obtained with two (B2), three (B3), and four (B4) nodes, respectively. The mathematical model can consist of several elements with different approximating degrees. On the other hand, the structural theory is developed by utilizing an arbitrary number (M) of functions $F_\tau(x, z)$. In this work, two polynomial bases are adopted to ap-

proximate the kinematic field, namely the Taylor and Lagrange expansion classes (denoted to as TE and LE). A generic N-order TE model (TEN) includes $M=\frac{(N+1)(N+2)}{2}$ power functions of the entire waveguide section coordinates. According to the LE approach, the section geometry is divided into a number of subdomains on which two-dimensional Lagrange functions are defined. The LE polynomial degree is determined by the number of nodes used to delimit each subdomain. Thus, bi-linear, bi-quadratic, and bi-cubic Lagrange functions are obtained with four (LE4), nine (LE9), and sixteen (LE16) nodes, respectively. The number of terms included in the kinematic field, M, is the total number of nodes belonging to the cross-section. The generalized coordinates of LE-based elements are only displacements, while TE models also encompass rotations and higher-order quantities. It should be highlighted that the FE discretization is not related to the sectional approximation; therefore, the segment length, Δ, can be selected arbitrarily. Instead, solid and plate FE models must fulfill the aspect-ratio condition of elements to perform reliably. Hence the discretizations along the three (or two) directions are mutually correlated. The use of Eq. 1 into a variational statement such as the Principle of Virtual Displacements or Hamilton's Principle leads to the so-called *fundamental nuclei* (FN) of FE matrices and vectors. Such operators are, for purely mechanical problems, 3-by-3 matrices and 3-by-1 vectors, whose components depend on neither the number of terms included in the kinematic expansion nor the class of approximating functions. Thanks to the indicial CUF formalism, motion equations corresponding to arbitrary kinematic fields of the waveguide segment can be derived with ease. The equations are

$$(\mathbf{K} + j\omega\mathbf{C} - \omega^2\mathbf{M})\mathbf{q} = \mathbf{F} \ ; \ \tilde{\mathbf{D}}(\omega)\mathbf{q} = \mathbf{F} \tag{2}$$

where $\mathbf{K}$, $\mathbf{C}$, and $\mathbf{M}$ are, respectively, the stiffness, damping, and mass matrices, $\mathbf{F}$ is the vector of the nodal forces, and $\mathbf{q}$ is the vector of the degrees of freedom. The matrix $\tilde{\mathbf{D}} = (\mathbf{K} + j\omega\mathbf{C} - \omega^2\mathbf{M})$ is, instead, the dynamic stiffness. It should be highlighted that Eq. 2 relies on the assumption that both forces and displacements are harmonic in time. It is possible to associate each term of matrices and vector in Eq. 2 to the left (L), right (R), and interior (I) nodes of the one-dimensional finite element model (see Fig. 1)

$$\begin{pmatrix} \tilde{\mathbf{D}}_{LL} & \tilde{\mathbf{D}}_{LI} & \tilde{\mathbf{D}}_{LR} \\ \tilde{\mathbf{D}}_{IL} & \tilde{\mathbf{D}}_{II} & \tilde{\mathbf{D}}_{IR} \\ \tilde{\mathbf{D}}_{RL} & \tilde{\mathbf{D}}_{RI} & \tilde{\mathbf{D}}_{RR} \end{pmatrix} \begin{pmatrix} \mathbf{q}_L \\ \mathbf{q}_I \\ \mathbf{q}_R \end{pmatrix} = \begin{pmatrix} \mathbf{F}_L \\ \mathbf{F}_I \\ \mathbf{F}_R \end{pmatrix} \tag{3}$$

If $\mathbf{F}_I = \mathbf{0}$, the system dimension can be reduced by expressing the interior degrees of freedom $\mathbf{q}_I$ in terms of $\mathbf{q}_L$ and $\mathbf{q}_R$. Thus, Eq. 2 becomes

$$\begin{pmatrix} \mathbf{D}_{LL} & \mathbf{D}_{LR} \\ \mathbf{D}_{RL} & \mathbf{D}_{RR} \end{pmatrix} \begin{pmatrix} \mathbf{q}_L \\ \mathbf{q}_R \end{pmatrix} = \begin{pmatrix} \mathbf{F}_L \\ \mathbf{F}_R \end{pmatrix} \tag{4}$$

Expressions of matrices $\mathbf{D}_{LL}$, $\mathbf{D}_{LR}$, $\mathbf{D}_{RL}$, and $\mathbf{D}_{RR}$ can be found in Ref. [24]. According to Bloch's theorem, the relation between the displacements and forces at the left and right sides of the periodic structure is

$$\begin{pmatrix} \mathbf{q}_R \\ \mathbf{F}_R \end{pmatrix} = \lambda_y \begin{pmatrix} \mathbf{q}_L \\ -\mathbf{F}_L \end{pmatrix} \quad \text{with} \quad \lambda_y = e^{-jk\Delta} \tag{5}$$

where k is the wavenumber, and the product (-$jk\Delta$) is the complex propagation constant. The periodic and equilibrium conditions for displacements and forces between two adjacent sections (denoted as $s1$ and $s2$) are

$$\begin{pmatrix} \mathbf{q}_R^{s1} \\ \mathbf{F}_R^{s1} \end{pmatrix} = \begin{pmatrix} \mathbf{q}_L^{s2} \\ -\mathbf{F}_L^{s2} \end{pmatrix} \tag{6}$$

By using Eqs. 4, 5, and 6, the dispersion problem becomes

$$\mathbf{T} \begin{pmatrix} \mathbf{q}_L \\ -\mathbf{F}_L \end{pmatrix} = \lambda_y \begin{pmatrix} \mathbf{q}_L \\ -\mathbf{F}_L \end{pmatrix} ; \mathbf{T} = \begin{pmatrix} -\mathbf{D}_{LR}^{-1}\mathbf{D}_{LL} & \mathbf{D}_{RL}^{-1} \\ -\mathbf{D}_{RL} + \mathbf{D}_{RR}\mathbf{D}_{LR}^{-1}\mathbf{D}_{LL} & -\mathbf{D}_{RR}\mathbf{D}_{LR}^{-1} \end{pmatrix} \tag{7}$$

where $\mathbf{T}$ is the transfer matrix. Equation 7 is solved for different propagation frequencies in order to calculate the eigenvalues λ_y, which are functions of the wavenumber k. Real eigenvalues correspond to propagating waves, imaginary ones to evanescent waves, while the complex values are related to attenuating waves. Eigenvectors collect coefficients to be used in the kinematic expansion for the computation of mode shapes and force distributions above the cross-section. If the left beam node has DOF_L degrees of freedom, the procedure requires the solution of a (2 DOF_L) system.
Alternatively, the dispersion problem can be posed by expressing the unknowns vector as follows

$$\begin{pmatrix} \mathbf{q}_L \\ \mathbf{q}_I \\ \mathbf{q}_R \end{pmatrix} = \mathbf{\Lambda}_R \begin{pmatrix} \mathbf{q}_L \\ \mathbf{q}_I \end{pmatrix} \; ; \; \mathbf{\Lambda}_R = \begin{pmatrix} \mathbf{I} & 0 \\ 0 & \mathbf{I} \\ \lambda_y \mathbf{I} & 0 \end{pmatrix} \tag{8}$$

where the identity sub-matrices can have different dimensions. If no external forces are exerted on the waveguide segment, the equilibrium conditions become

$$\mathbf{\Lambda}_L \begin{pmatrix} \mathbf{F}_L \\ \mathbf{F}_I \\ \mathbf{F}_R \end{pmatrix} = \mathbf{0} \, ; \, \mathbf{\Lambda}_L = \begin{pmatrix} \mathbf{I} & 0 & 0 \\ 0 & \mathbf{I} & \lambda_y^{-1} \mathbf{I} \end{pmatrix} \tag{9}$$

Substituting Eqs. 8 and 9 in Eq. 2, equations of motion are as follow

$$(\mathbf{\Lambda}_L \mathbf{K} \mathbf{\Lambda}_R + j\omega \mathbf{\Lambda}_L \mathbf{C} \mathbf{\Lambda}_R - \omega^2 \mathbf{\Lambda}_L \mathbf{M} \mathbf{\Lambda}_R) \bar{\mathbf{q}} = \mathbf{0} \tag{10}$$

where $\bar{\mathbf{q}} = (\mathbf{q}_L \, \mathbf{q}_I)^{\mathrm{T}}$. Equation 10 provides propagation frequencies at which wave modes propagate for given wavenumbers. Since inputs for the analysis are purely real propagation constants, the resulting dispersion characteristics are related to propagating waves only. The system dimension is, in this case, (DOF_L+DOF_I) where DOF_I refers to the internal degrees of freedom.

3. Numerical results

The following section presents the dispersion diagrams on the $\omega\,(f) - k$ plane of different one-dimensional waveguides. The mixed interpolation of tensorial component formulation has been adopted to mitigate potential shear locking issues due to the finite element approximation.

3.1. Dispersion curves of compact rectangular cross-sections: isotropic and sandwich cases

The first numerical applications concerned a rectangular cross-section, which was 0.116 mm wide and 0.055 mm thick. For the isotropic case, the Young modulus, Poisson's ratio, and density were assumed equal to 9.8 Gpa, 0.3, and 1580 kg m^{-1}. This simple configuration was considered to investigate the effects of the kinematics and the finite beam element order on dispersion characteristics' computation. Figure 2 shows the frequency spectra of two

waveguides obtained with different FE discretizations and the same kinematic theory, namely the first-order Taylor-type expansion (TE1). For $\Delta =$ 0.02 m and wavenumbers larger than 40 rad m^{-1}, the propagation curves predicted by the model consisting of a single finite linear element (1-B2) differ from those obtained with higher-order formulations (1-B3 and 1-B4). Although the mesh refinement with two (2-B2) and three 2-node (3-B2) elements lessened such discrepancies, the use of higher-order FE is advantageous from the computational perspective since the 2-B2 and 3-B2 models have the same numbers of degrees of freedom of the 1-B3 and 1-B4 discretizations, respectively. For the shortest segment ($\Delta = 0.002$ m), the various FE models provided the same results within the considered wavenumber interval.

On the other hand, Fig. 3 compares the frequency spectra calculated with the second-, third-, and fifth-order Taylor-like expansions by utilizing 1-B2 along the waveguide axis. Differently to what was observed for the TE1 theory, which only detected propagating and evanescence waves, advanced kinematics enabled attenuating waves (red dots in the graphs) to be characterized.

Apart from detecting new wave modes, the rising of the theory order led to shifts of curves related to propagating waves toward lower frequencies. Figure 4 aims at showing such an effect by comparing results obtained with the second- and fifth-order Taylor-type theories. The section deformations corresponding to these dispersion curves are shown in Fig. 5.

As far as the sandwich configuration is concerned, the waveguide was assumed to be made up of a soft-core 50 mm thick embedded between two stiff layers with a thickness equal to 2.5 mm each. Material properties of the skin layers were $E = 9.8$ GPa, $\nu = 0.3$ and $\rho = 1580$ kg m^{-3} while those of the core were assumed equal to $E = 0.094$ GPa, $\nu = 0.3$ and $\rho = 101$ kg m^{-3}. The waveguide portion was 2 mm long, and one linear finite beam element was utilized along the propagation direction. Figure 6 shows the dispersion curves of two propagating wave modes computed with various Taylor-like models and a Lagrange-type solution. The LE kinematics was obtained by discretizing the cross-section with ten 9-node Lagrange elements (10-LE9); Two and three LE elements were utilized along the thickness direction for the skin layers and the core, while two elements were used along the width.

For comparison purposes, the graph reports the 3D finite element solution presented in Ref. [41]. The significant transversal anisotropy of the section required refined kinematics to describe the wave propagation mechanisms adequately. From the zoom-in picture, it is possible to observe how the order

increasing allowed the 3D solution to be approximated more and more accurately. Moreover, it is interesting to note that the third- and fourth-order TE theories predicted negative group velocities ($\boldsymbol{d}\omega\ /\boldsymbol{d}k$) of the compressional wave for $4000 < frequency < 5000$ Hz, while the remaining CUF theories and the reference solution provided positive values. Figures 7 shows dispersion curves corresponding to high-order wave modes computed with the LE model. Apart from mode shapes dominated by flexural, axial, and torsional displacements, the CUF solution allowed one to capture thickness deformations, as illustrated in Fig. 8.

3.2. Dispersion curves of a box beam

The structure had outer dimensions, and the wall thickness equal to 102, 52, and 2 mm, respectively. The material was an aluminum with $E = 71$ GPa, $\nu = 0.33$, and $\rho = 2700$ kg m^{-1}. The portion considered for numerical simulations (1 mm long) was discretized by utilizing one linear beam element (1-B2), while the cross-section was modeled with the Lagrange-type solutions, schematically depicted in Fig. 9.

Curves related to flexural, torsional, axial, and shell-type mode shapes are shown in Fig. 10. Moreover, results obtained with a two-dimensional FE model consisting of five *CQUAD4* elements per edge [19] are reported for comparison purposes.

CUF solutions provided comparable results for flexural modes about the z-axis (curves (b) and (h)), the axial (curve (d)), and torsional (curve (c)) wave modes. Branch variations related to other waves, instead, differ significantly. Shell-type/torsional (S/T), pumping (P) and shell-type/flexural (S/F$_x$ and S/F$_z$) distortions are illustrated in Fig. 11 together with the corresponding cut-on frequencies.

The refined mesh determined cut-on frequencies reductions of roughly 7, 11, and 40% for the S/T, P, and S/F$_x$ deformations. For the flexural wave mode about the x-axis (curve (a)), the two models significantly differ for wavenumbers larger than 10 rad s^{-1}. Dispersion curves obtained with the present approach generally have higher slopes (wavenumbers increase more rapidly with the frequency) than those proposed in the reference paper. Such a discrepancy could be ascribed to two factors: 1) the different edge kinematics descriptions of the two approaches, and 2) the 2D mesh convergence. As far as the first aspect is concerned, the structure contour is moderately thick; therefore, a linear kinematic assumption along the thickness could not be enough to detect in- and out-of-plane warpings of edges, especially for

short wavelengths. The second observation can be justified by merely comparing the cut-on frequencies obtained with the plate and 1D-CUF solutions. Figure 12 illustrates real and imaginary wave modes at different wavenumbers corresponding to curves (a) and (b) of Fig. 10.

For wavenumbers lower than approximately 10 rad s^{-1}, flexural waves are dominated by section rigid transverse motions, while edge deformations become more and more detectable as the propagating frequency increases. From Fig. 10, it is possible to observe that branches (a) and (b) veer and rapidly diverge away within the interval $10< k <20$, namely, when they approach the curves (f) and (g). For larger wavenumbers ($k > 20$), the real wave modes have similarities with the coupled shell/flexural deformations of Fig. 11, while imaginary eigenmodes exhibit significant out-of-plane warpings.

4. Conclusion

This paper assessed the capabilities of high-order beam elements in calculating the dispersion characteristics of various one-dimensional waveguides. Stiffness and mass matrices of a finite waveguide portion were computed with a unified formalism and used to build the transfer matrices according to the WFE method. Simulations were performed on compact isotropic and sandwich waveguides and a metallic box beam with a moderately-thick contour. The finite element discretization was exploited along the wave propagation direction, while expansions based on Taylor- and Lagrange-like polynomials were adopted to approximate the displacement field above the waveguide section. Results revealed that higher-order functions along the propagation direction provided convergent results for wider wavenumber intervals than models with the same degrees of freedom consisting of linear elements. Moreover, the use of advanced theories allowed one to detect higher-order wave modes, which involved in- and out-of-plane warpings of the cross-section. The finite beam element dimension does not influence the cross-section kinematic model; therefore, arbitrary lengths of waveguide segment can be modeled with roughly the same number of degrees of freedom. The 3D-FE approach does not present such a feature since the elements aspect-ratio constraint must be fulfilled along the three spatial directions to provide reliable results. The 1D-CUF approach can be considered a reliable and viable alternative to 2D and 3D finite element solutions for computing dispersion characteristics of complex waveguides.

Acknowledgments

The authors would like to acknowledge the DEVISU project, supported by the *Ministero dell'Istruzione, dell'Universitá della Ricerca* research funding programme PRIN 2017.

Declaration of Interest statement

The authors declare that they have no conflict of interest.

References

[1] karl F. Graff. *Wave motion in elastic solids*. Dover Publication, 1991.

[2] JR Banerjee. Free vibration analysis of a twisted beam using the dynamic stiffness method. *International Journal of Solids and Structures*, 38(38-39):6703–6722, 2001.

[3] JR Banerjee. Development of an exact dynamic stiffness matrix for freevibration analysis of a twisted timoshenko beam. *Journal of Sound and Vibration*, (270):379–401, 2004.

[4] M. Boscolo and J.R. Banerjee. Dynamic stiffness method for exact in-plane freevibration analysis of plates and plate assemblies. *Journal of Sound and Vibration*, 330(12):2928–36, June 2011.

[5] F.A. Fazzolari, Boscolo M., and JR. Banerjee. An exact dynamic stiffness element using a higher order shear deformation theoryfor free vibration analysis of composite plate assemblies. *Composite Structures*, 96:262–278, 2013.

[6] Pagani A., M. Boscolo, J.R. Banerjee, and E. Carrera. Exact dynamic stiffness elements based on one-dimensional higher-order theories for free vibration analysis of solid and thin-walled structures. *Journal of Sound and Vibration*, 332:6104–27, 2013.

[7] James F Doyle. *Wave propagation in structures: an FFT-based spectral analysis methodology*. Springer Science & Business Media, 2012.

[8] Massimo Ruzzene. Vibration and sound radiation of sandwich beams with honeycomb truss core. *Journal of sound and vibration*, 277(4-5):741–763, 2004.

[9] D Roy Mahapatra and S Gopalakrishnan. A spectral finite element model for analysis of axial–flexural–shear coupled wave propagation in laminated composite beams. *Composite Structures*, 59(1):67–88, 2003.

[10] A Chakraborty and S Gopalakrishnan. A spectral finite element model for wave propagation analysis in laminated composite plate. *Journal of Vibration and Acoustics*, 128(4):477–488, 2006.

[11] Dimitri Komatitsch, Christophe Barnes, and Jeroen Tromp. Simulation of anisotropic wave propagation based upon a spectral element method. *Geophysics*, 65(4):1251–1260, 2000.

[12] Haikuo Peng, Guang Meng, and Fucai Li. Modeling of wave propagation in plate structures using three-dimensional spectral element method for damage detection. *Journal of Sound and Vibration*, 320(4-5):942–954, 2009.

[13] Paweł Kudela, Arkadiusz Żak, Marek Krawczuk, and Wiesław Ostachowicz. Modelling of wave propagation in composite plates using the time domain spectral element method. *Journal of Sound and Vibration*, 302(4-5):728–745, 2007.

[14] AG de Miguel, A Pagani, and E Carrera. Higher-order structural theories for transient analysis of multi-mode lamb waves with applications to damage detection. *Journal of Sound and Vibration*, 457:139–155, 2019.

[15] L Gavrić. Finite element computation of dispersion properties of thin-walled waveguides. *Journal of sound and vibration*, 173(1):113–124, 1994.

[16] Vitali V Volovoi, Dewey H Hodges, Victor L Berdichevsky, and Vladislav G Sutyrin. Dynamic dispersion curves for non-homogeneous, anisotropic beams with cross-sections of arbitrary geometry. *Journal of Sound and Vibration*, 215(5):1101–1120, 1998.

[17] Hauke Gravenkamp, Chongmin Song, and Jens Prager. A numerical approach for the computation of dispersion relations for plate structures using the scaled boundary finite element method. *Journal of sound and vibration*, 331(11):2543–2557, 2012.

[18] Hauke Gravenkamp, Hou Man, Chongmin Song, and Jens Prager. The computation of dispersion relations for three-dimensional elastic waveguides using the scaled boundary finite element method. *Journal of Sound and Vibration*, 332(15):3756–3771, 2013.

[19] L Houillon, MN Ichchou, and L Jezequel. Wave motion in thin-walled structures. *Journal of Sound and Vibration*, 281(3-5):483–507, 2005.

[20] M. N. Ichchou, S. Akrout, and J.-M. Mencik. Guided waves group and energy velocities via finite elements. *Journal of sound and Vibration*, 305:931–944, 2007.

[21] Y Waki, BR Mace, and MJ Brennan. Free and forced vibrations of a tyre using a wave/finite element approach. *Journal of Sound and Vibration*, 323(3-5):737–756, 2009.

[22] J-M Mencik and MN Ichchou. Wave finite elements in guided elastodynamics with internal fluid. *International Journal of Solids and Structures*, 44(7-8):2148–2167, 2007.

[23] Massimo Ruzzene, Luca Mazzarella, Panagiotis Tsopelas, and Fabrizio Scarpa. Wave propagation in sandwich plates with periodic auxetic core. *Journal of Intelligent Material Systems and Structures*, 13:587–597, September 2002.

[24] Brian R Mace, Denis Duhamel, Michael J Brennan, and Lars Hinke. Finite element prediction of wave motion in structural waveguides. *The Journal of the Acoustical Society of America*, 117(5):2835–2843, 2005.

[25] Brian R. Mace and Elisabetta Manconi. Modelling wave propagation in two-dimensional structures using finite element analysis. *Journal of Sound and Vibration*, 318:884–902, 2008.

[26] Elisabetta Manconi and Sergey Sorokin. On the effect of damping on dispersion curves in plates. *International Journal of Solids and Structures*, 50:1966–1973, 2013.

[27] M. L. Accorsi and M. S. Bennett. A finite element based method for the analysis of free wave propagation in stiffened cylinders. *Journal of Sound and Vibration*, 148:279–292, 1991.

[28] M. Collet, M. Ouisse, M. Ruzzene, and M. N. Ichchou. Floquet - bloch decomposition for the computation of dispersion of two-dimensional periodic, damped mechanical systems. *International Journal of Solids and Structures*, 48:2837–2848, 2011.

[29] Parthkumar G. Domadiya, Elisabetta Manconi, Marcello Vanali, Lars V. Andersen, and Andrea Ricci. Numerical and experimental investigation

of stop-bands in finite and infinite periodic one-dimensional structures. *Journal of Vibration and Control*, 22:920–931, 2016.

[30] D. Beli, J. R. F. Arruda, and M. Ruzzene. Wave propagation in elastic metamaterial beams and plates with interconnected resonators. *International Journal of Solids and Structures*, 139-140:105–120, 2018.

[31] S. Timorian, G. Petrone, S. De Rosa, F. Franco, M. Ouisse, and N. Bouhaddi. Proceedings of the institution of mechanical engineers, part c: Journal of mechanical engineering science. *Journal of Mechanical Engineering Science*, 233:7498–7512, 2019.

[32] E. Carrera and M. Petrolo. Refined one-dimensional formulations for laminated structure analysis. *AIAA journal*, 50:176–189, 2012.

[33] B Wu, A Pagani, M Filippi, WQ Chen, and E Carrera. Accurate stress fields of post-buckled laminated composite beams accounting for various kinematics. *International Journal of Non-Linear Mechanics*, 111:60–71, 2019.

[34] E. Carrera, E. Zappino, and M. Petrolo. Analysis of thin-walled structures with longitudinal and transversal stiffeners. *Journal of Applied Mechanics*, 80:011006 (12 pages), 2013.

[35] E. Carrera, A. Pagani, and M. Petrolo. Component-wise method applied to vibration of wing structures. *Journal of Applied Mechanics*, 80, 2013.

[36] E. Carrera and M. Filippi. A refined one-dimensional rotordynamics model with three-dimensional capabilities. *Journal of Sound and Vibration*, 366:343–356, 2016.

[37] M. Filippi, A. Pagani, and E. Carrera. Accurate nonlinear dynamics and mode aberration of rotating blades. *Journal of Applied Mechanics*, 85, 2018.

[38] A. Entezari, M. Filippi, and E. Carrera. Unified finite element approach for generalized coupled thermoelastic analysis of 3d beam-type structures, part 1: Equations and formulation. *Journal of Thermal Stresses*, 40:1386–1401, 2017.

[39] Ayoob Entezari, Matteo Filippi, Erasmo Carrera, and Mohammad Ali Kouchakzadeh. 3d-wave propagation in generalized thermoelastic functionally graded disks. *Composite Structures*, 206:941–951, 2018.

[40] Erasmo Carrera, Maria Cinefra, Marco Petrolo, and Enrico Zappino. *Finite element analysis of structures through unified formulation*. John Wiley & Sons, 2014.

[41] Vincenzo D'Alessandro. *Investigation and assessment of the wave and finite element method for structural waveguides*. PhD thesis, University of Naples Federico II, March 2014.

Figure

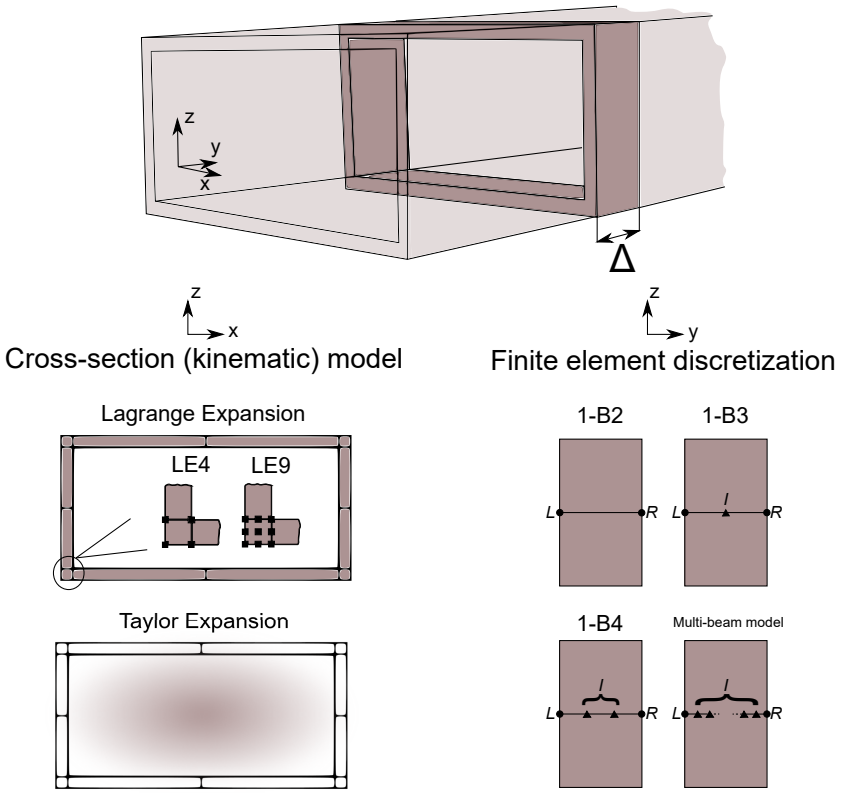

Figure 1: Sketch of a one-dimensional waveguide. Structural and mathematical CUF model.

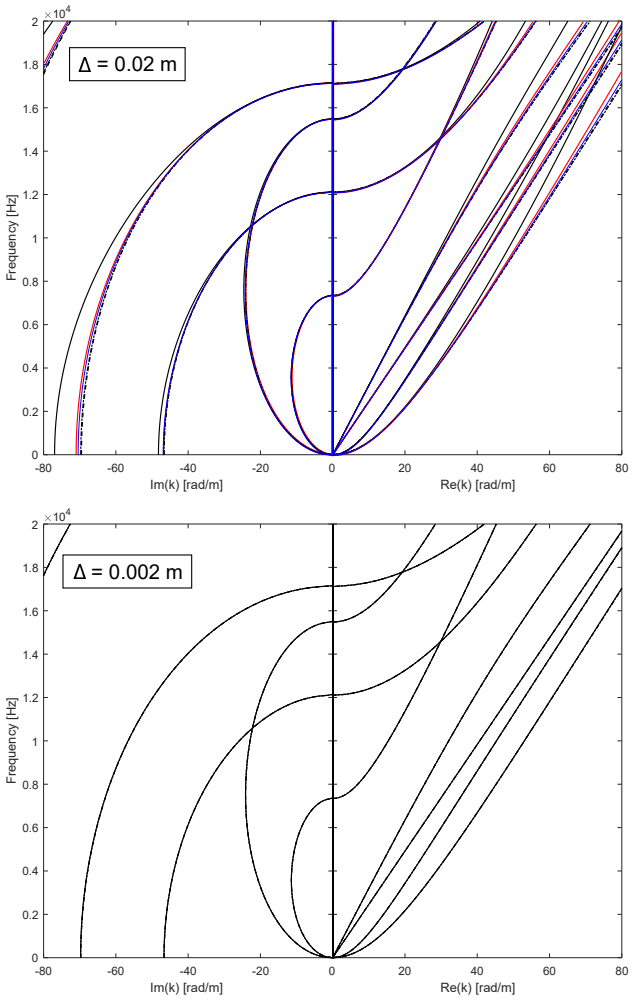

Figure 2: Curves related to propagating and evanescence waves of the isotropic rectangular section. Continuous black curves: 1-B2; continuous red curves: 2-B2; continuous blue curves: 3-B2; Dashed curves: 1-B3; Line-dot curves: 1-B4. Used kinematic theory: TE1.

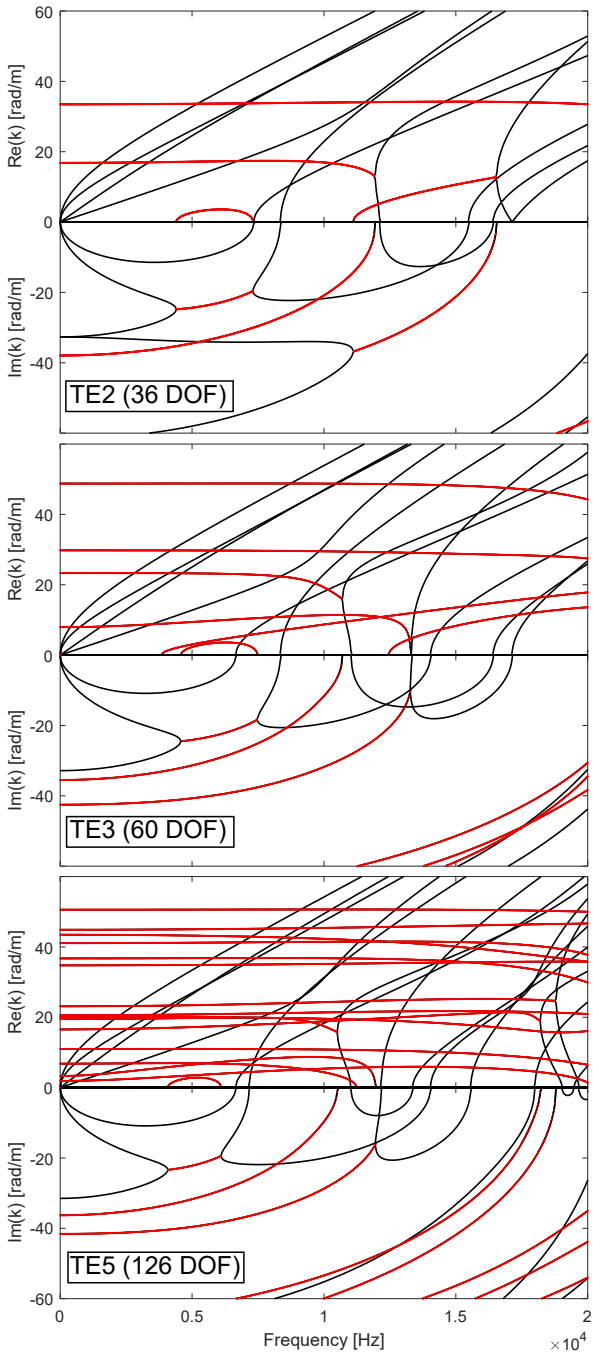

Figure 3: Curves related to propagating, evanescence and attenuating waves of the isotropic rectangular section. Continuous black curves: propagating and evanescence waves; red dots: attenuating waves. $\Delta = 0.002$ m; FE discretization: 1-B2.

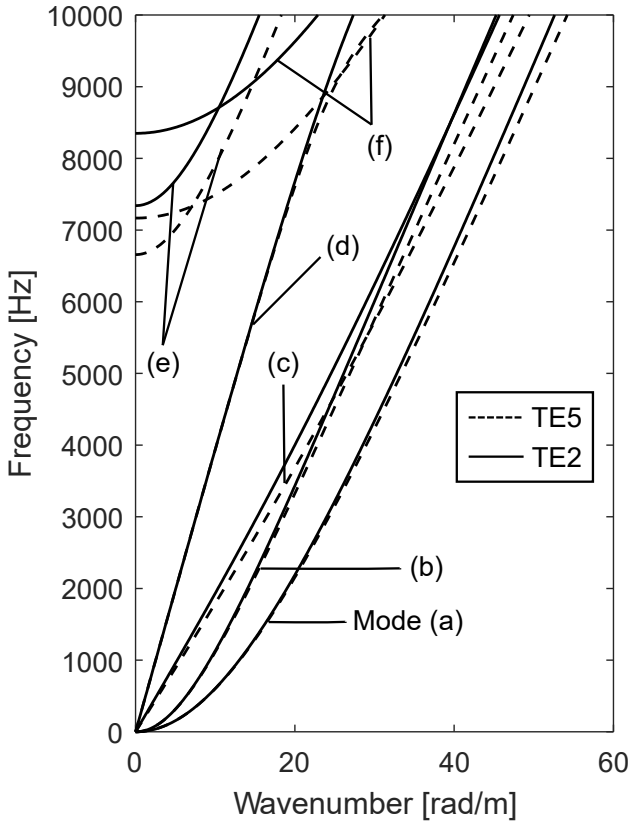

Figure 4: Disperison curves related to propagating waves of the isotropic rectangular section. $\Delta = 0.002$ m; FE discretization: 1-B2.

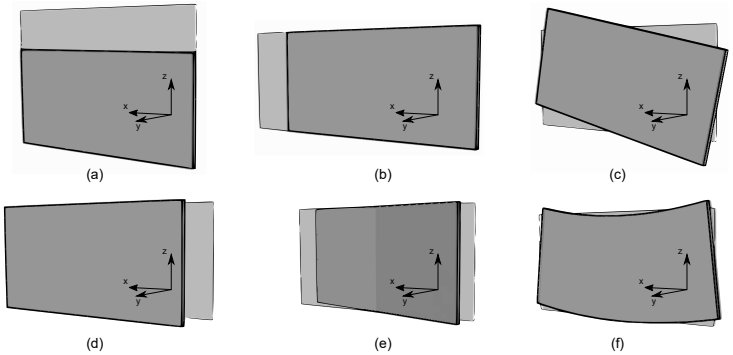

Figure 5: Wavemodes corresponding to the dispersion curves of Fig. 4.

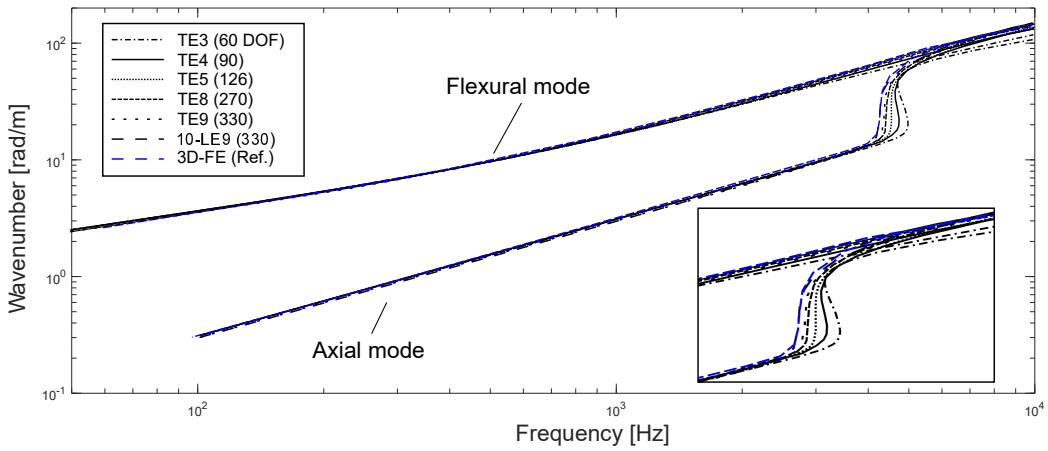

Figure 6: Dispersion curves of the sandwich beam for two propagating waves. The values in parenthesis is the number of degrees of freedom.

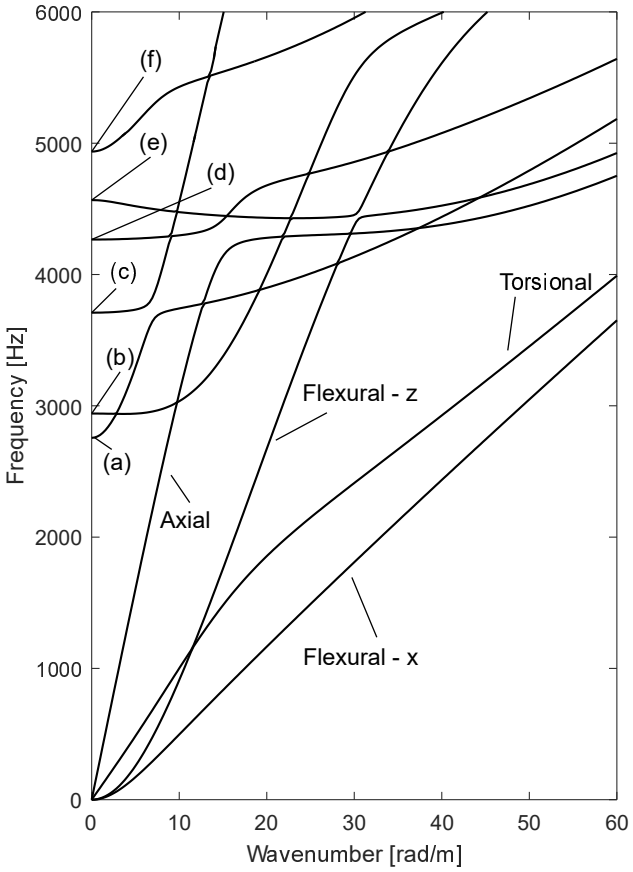

Figure 7: Disperison curves related to the first ten propagating waves of the sandwich rectangular section. $\Delta = 0.002$ m; FE discretization: 1-B2, kinematic model: 10-LE9.

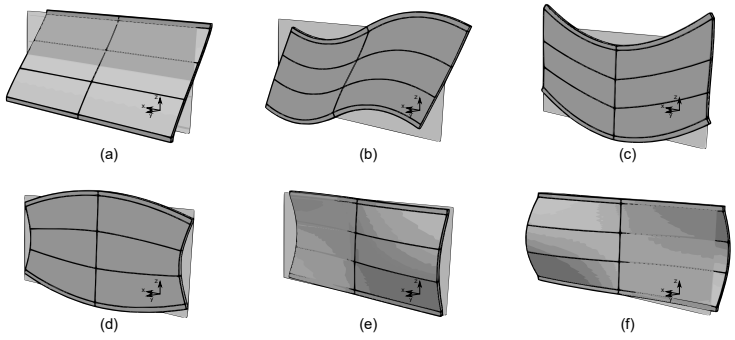

Figure 8: Higher-order wave modes related to the frequency spectrum of Fig. 7. Cut-on frequencies: (a) 2755.9; (b) 2941.3; (c) 3709.4; (d) 4266.4; ; (e) 4566.9; (f) 4936.2 Hz.

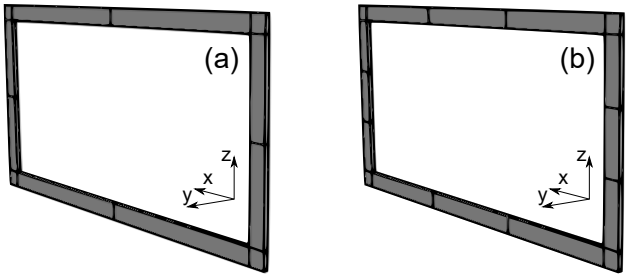

Figure 9: LE models of the box beam: (a) 12-LE9 (432 DOF); (b) 16-LE9 (576 DOF).

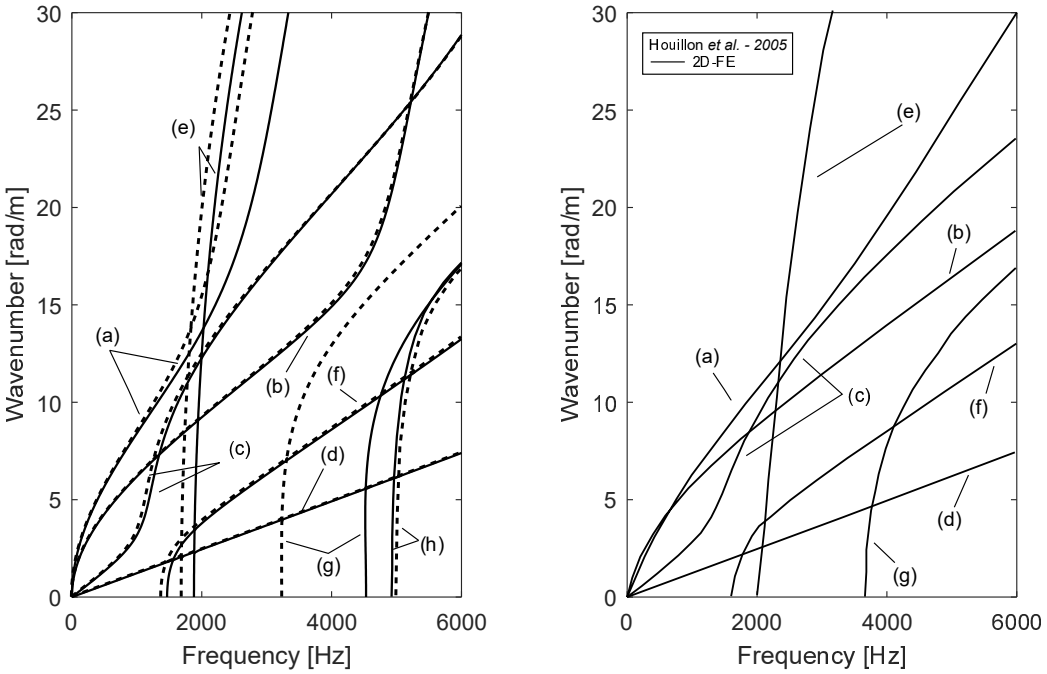

Figure 10: Dispersion curves of a box metallic beam computed with 12-LE9 (solid curves) and 16-LE9 (dashed curves) models. Wave modes: (a) flexural - x; (b) flexural - z; (c) torsional; (d) axial; (e) pumping; (f) shell-type/torsional; (g) shell-type/flexural-x; (h) shell-type/flexural-z.

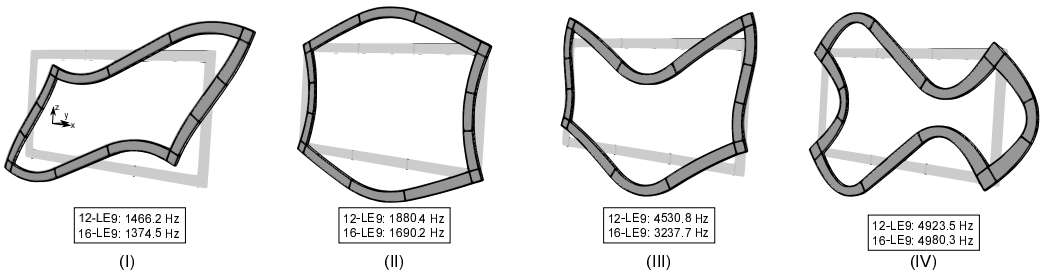

Figure 11: Wave modes of the box beam and related cut-on frequencies. I) Shell-like/torsional (S/T), II) pumping (P), III) Shell-like/flexural about the x-axis (S/F$_x$) and IV) Shell-like/flexural about the z-axis $_z$.

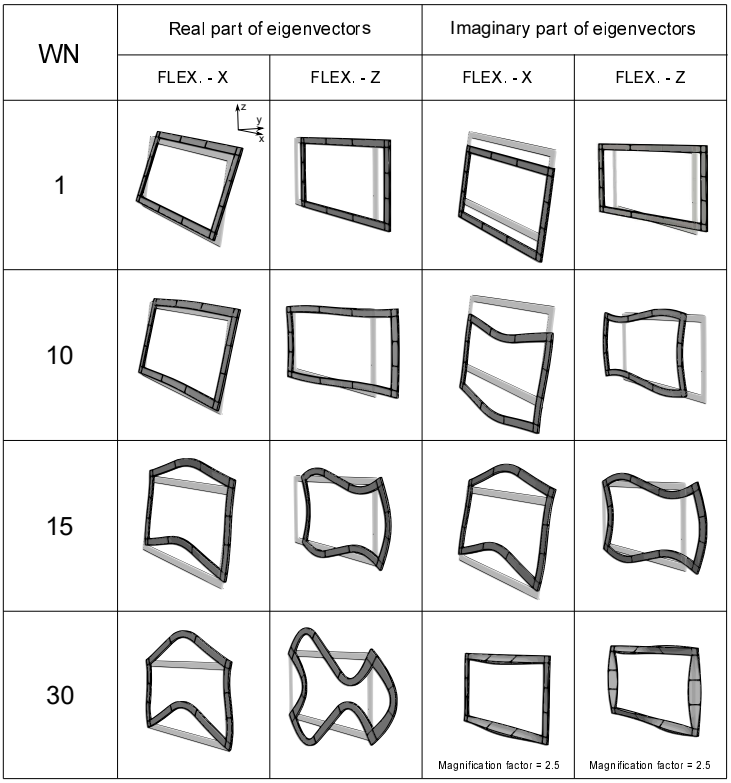

Figure 12: Flexural wave modes as functions of the wavenumber. Both real and imaginary parts are adimensionalized with respect to the maximum wavevector module.

List of Figures